Eur. J. Mineral., 36, 797–811, 2024
https://doi.org/10.5194/ejm-36-797-2024
© Author(s) 2024. This work is distributed under
the Creative Commons Attribution 4.0 License.

European Journal of Mineralogy
Open Access

Crystal chemistry of K-tourmalines from the Kumdy-Kol microdiamond deposit, Kokchetav Massif, Kazakhstan

Beatrice Celata[1,2], Ferdinando Bosi[1], Kira A. Musiyachenko[3,4], Andrey V. Korsakov[3], and Giovanni B. Andreozzi[1]

[1]Department of Earth Sciences, Sapienza University of Rome, Piazzale Aldo Moro 5, 00185 Rome, Italy
[2]Department of Energy Technologies and Renewable Sources, ENEA Casaccia Research Center, S. Maria di Galeria, 00123 Rome, Italy
[3]Sobolev Institute of Geology and Mineralogy, Siberian Branch of the Russian Academy of Sciences (RAS), Novosibirsk, Russian Federation
[4]Department of Earth, Ocean and Atmospheric Sciences, University of British Columbia, Vancouver, V6T, Canada

Correspondence: Beatrice Celata (beatrice.celata@enea.it) and Ferdinando Bosi (ferdinando.bosi@uniroma1.it)

Received: 10 January 2024 – Revised: 12 June 2024 – Accepted: 22 June 2024 – Published: 12 September 2024

Abstract. Selected crystals of natural K-bearing tourmalines, extracted from a quartzofeldspathic rock from the Kumdy-Kol microdiamond deposit (an ultrahigh-pressure region of Kokchetav Massif, northern Kazakhstan), were characterized using a scanning electron microscope, an electron microprobe and single-crystal X-ray diffraction to investigate the impact of K uptake on the tourmaline structure.

All the studied crystals belong to the maruyamaite–oxy-dravite/dravite compositional field, with K contents ranging from 0.03 to 0.47 apfu (atoms per formula unit), and contain a minor fluor-uvite component that increases towards oxy-dravite and dravite. The compositional variability of our samples can be expressed as a sequence of substitutions ranging from maruyamaite to oxy-dravite, dravite and fluor-uvite (or vice versa). Specifically, the substitutions that lead from maruyamaite to oxy-dravite to dravite are (1) $^{X}\mathrm{K} + \mathrm{Al}_{\mathrm{TOT}} + {}^{\mathrm{O1}}\mathrm{O} \leftrightarrow {}^{X}\mathrm{Na} + \mathrm{Mg}_{\mathrm{TOT}} + {}^{\mathrm{O1}}\mathrm{O}$ and (2) $^{X}\mathrm{Na} + \mathrm{Mg}_{\mathrm{TOT}} + {}^{\mathrm{O1}}\mathrm{O} \leftrightarrow {}^{X}\mathrm{Na} + \mathrm{Mg}_{\mathrm{TOT}} + {}^{\mathrm{O1}}\mathrm{OH}$, respectively. Conversely, the substitutions that lead from oxy-dravite to dravite to fluor-uvite are (1) $^{X}\mathrm{Na} + \mathrm{Mg}_{\mathrm{TOT}} + {}^{\mathrm{O1}}\mathrm{O} \leftrightarrow {}^{X}\mathrm{Na} + \mathrm{Mg}_{\mathrm{TOT}} + {}^{\mathrm{O1}}\mathrm{OH}$ and (2) $^{X}\mathrm{Na} + \mathrm{Mg}_{\mathrm{TOT}} + {}^{\mathrm{O1}}\mathrm{OH} \leftrightarrow {}^{X}\mathrm{Ca} + \mathrm{Mg}_{\mathrm{TOT}} + {}^{\mathrm{O1}}\mathrm{F}$, respectively.

By analysing the difference between the bond valence sum and mean formal charge at the X site, we show that an increase in the K content ($\mathrm{K} > 0.21$ apfu) results in the compression of X–O bonds (overbonded cation). Conversely, lower K contents lead to the stretching of the bonds (underbonded cation). Compared to the K-dominant analogues with $^{Z}\mathrm{FeO}_6$ povondraite-type framework, K-bearing tourmalines with a smaller $^{Z}\mathrm{AlO}_6$ framework such as maruyamaite should only be stable at higher-pressure conditions, as pressure is necessary to squeeze the relatively large K cation into the tighter X cavity. In both cases, the essential condition for the formation of K-dominant tourmalines is the extremely high K activity in the crystallization fluid. The K-tourmaline from the Kokchetav Massif may have crystallized under high-pressure (HP) conditions, with an upper limit between 3.5–7 GPa, during retrograde metamorphism following the ultrahigh-pressure (UHP) metamorphic peak.

1 Introduction

During partial melting and devolatilization of mantle peridotites and subducted crustal material, potassium (K), which is an incompatible element owing to its large size, strongly partitions into the melts and fluids released (e.g. Schmidt, 1996; Thomsen and Schmidt, 2008; Hermann and Green, 2001; Hermann et al., 2006a). In subduction zones, potential carriers of water, boron and potassium, such as sanidine, phlogopite and K-bearing amphiboles, have been intensively studied (see Harlow and Davies, 2004). However, the role of tourmaline, often considered restricted to shallower geological settings (Henry and Dutrow, 1992), has been underestimated. Contrary to this belief, tourmaline's stability field is extensive, as tourmaline crystallizes in a variety of geological settings, representing the most important boron rock-forming mineral from the surface of the crust to the upper mantle (e.g. Marschall et al., 2009; Lussier et al., 2016).

Tourmalines are a mineral supergroup of complex borosilicates, listed among the earliest Li-minerals that made their first appearance on Earth (Grew et al., 2016). Extensive research into their structure and chemistry has revealed their adaptability to host a variety of elements, contributing to their stability across a wide range of pressures and temperatures (Bosi, 2018; Dutrow and Henry, 2011; van Hinsberg et al., 2011). This peculiar feature is revealed by its general formula: $XY_3Z_6T_6O_{18}(BO_3)_3V_3W$, where, commonly, X represents Na^+, K^+, Ca^{2+}, or □ (which equals vacancy); Y represents Al^{3+}, Cr^{3+}, V^{3+}, $Fe^{2+/3+}$, Mg^{2+}, Mn^{2+}, Li^+, or Ti^{4+}; *Z* represents Al^{3+}, Cr^{3+}, V^{3+}, $Fe^{2+/3+}$, or Mg^{2+}; T represents Si^{4+}, Al^{3+}, or B^{3+}; B represents B^{3+}; V represents $(OH)^-$ or O^{2-}; and W represents $(OH)^-$, F^-, or O^{2-}. When not italicized, letters represent groups of constituents at the $^{[9]}X$, $^{[6]}Y$, $^{[6]}Z$, $^{[4]}T$, and $^{[3]}B$ crystallographic sites (letters italicized). When groups of anions are located at the $^{[3]}$O3 and $^{[3]}$O1 sites, letters V and W are respectively used. Hydrogen atoms occupy the H3 and H1 sites, which are linked to O3 and O1, respectively. Based on *X* site dominant occupancy, tourmalines can be primarily classified as vacant, alkali and calcic (Henry et al., 2011).

Tourmalines with the *X* site partially occupied by K have been reported from two distinctive localities so far: the Kokchetav Massif, northern Kazakhstan (Shimizu and Ogasawara, 2005, 2013), and Bolivia, Cochabamba region (Walenta and Dunn, 1979). In the first case, the K-dominant tourmaline was approved as the new species maruyamaite: $K(MgAl_2)(Al_5Mg)Si_6O_{18}(BO_3)_3(OH)_3O$ (Lussier et al., 2016). In the second case, the K-bearing tourmaline from Bolivia was first approved as the new species feruidravite (Walenta and Dunn, 1979) and then renamed as povondraite, $NaFe^{3+}_3(Fe^{3+}_4Mg_2)Si_6O_{18}(BO_3)_3(OH)_3O$ (Grice et al., 1993). The same authors also found a zoned sample having a povondraite core rimmed by a tourmaline containing up to 0.56 K per formula unit (pfu). These povondraite samples occur in a meta-evaporite, probably Cambrian in age, known as the Locotal Breccia in Alto Chapare, Cochabamba Department, central Bolivian Andes (Žáček et al., 1998). The crystal chemistry of these samples has been extensively studied by Žáček et al. (1998, 2000) and Bosi et al. (2023).

This paper focuses on K-bearing and K-dominant tourmaline samples from the Kumdy-Kol microdiamond deposit (Kokchetav Massif, Kazakhstan). It has been suggested that the K-dominant composition of maruyamaite could be attributed to the relatively high *P*–*T* conditions of its crystallization. In fact, findings of microdiamond inclusions in both maruyamaite and K-bearing oxy-dravite crystals from quartz-feldspathic gneisses of the Kumdy-Kol area led to the hypothesis of the ultrahigh-pressure (UHP) formation conditions of this assemblage (Shimizu and Ogasawara, 2005, 2013). The UHP conditions are thought to facilitate K accommodation at the *X* site, as K is so large that it would need to be squeezed at high pressure to enter the site (Shimizu and Ogasawara, 2005, 2013; Ota et al., 2008).

However, the genesis of maruyamaite in UHP environments is still under debate. Berryman et al. (2014, 2015) and Marschall et al. (2009) suggested that the absence of Na as a competitor for the *X* site occupancy during tourmaline formation is crucial for the uptake of the otherwise disfavoured K cation. A new occurrence of maruyamaite in the Barchi-Kol site (Musiyachenko et al., 2021) led to the suggestion that high K activity in the forming environment rather than the pressure alone controls the final composition of the phase (Safonov et al., 2011). Moreover, tourmaline from UHP terrains typically does not exhibit comparable K contents, only showing K contents up to 0.05 apfu (atoms per formula unit; see Ertl et al., 2010).

Experimental work by Berryman et al. (2015) demonstrated that the occupancy of K at the *X* site increases with pressure almost linearly in a Na-free fluid, indicating that a pressure higher than 2 GPa is necessary to achieve the high K occupancy found in natural maruyamaite samples from the Kokchetav Massif. High-pressure experimental work performed on maruyamaite by Likhacheva et al. (2019) demonstrated a stabilizing function of K at $P > 15$ GPa and an overall structural resistance up to 20 GPa, irrespective of the role of temperature, which was not investigated.

These findings suggest that K-rich tourmalines could transport K down to the upper mantle, where it could be hosted by nominally anhydrous phases and further transported to deeper parts of the mantle, as documented by findings of high K_2O contents in clinopyroxene in diamondiferous eclogites (Mikhailenko et al., 2020, 2021) and inclusions in diamonds from South African and Yakutian kimberlites (Erlank and Kushiro, 1970; Sobolev, 1977; Prinz et al., 1975; Bishop et al., 1978). For nominally anhydrous phases, an important role of pressure for K to be accommodated into the crystal structure was observed, specifically for garnet at $P > 20$ GPa (e.g. Wang and Takahashi, 1999). Therefore, the structural characterization of both K-rich and K-poor tour-

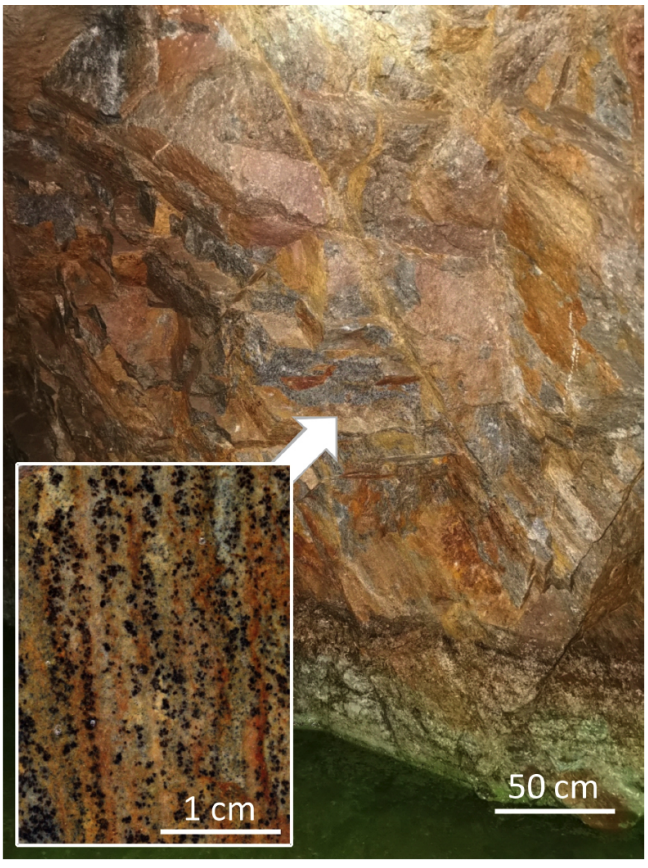

Figure 1. Photo of outcrop of K-bearing tourmalines in the main gallery of the Kumdy-Kol microdiamond deposit. Insert: slab of K-bearing tourmaline sample.

maline is important for enhancing our understanding of how K can be incorporated at the *X* site and how the structure adapts to this unusual composition.

In the present study, nine samples of natural K-bearing tourmalines from the Kumdy-Kol microdiamond deposit were characterized using scanning electron microscopy (SEM), an electron microprobe (EMP) and single-crystal X-ray diffraction (SC-XRD). This investigation aimed to explore their crystal chemistry and the structural consequences of incorporating increasing amounts of K.

Geological setting

The Kokchetav Massif (northern Kazakhstan) is located within one of the largest suture zones, namely the Caledonian Central Asian fold belt (Zonenshain et al., 1990; Dobretsov et al., 1995). This area is well known due to abundant findings of diamond and coesite-bearing metamorphic rocks (Sobolev and Shatsky, 1990; Sobolev et al., 1991; Shimizu and Ogasawara, 2005). The origin of the Kokchetav Massif is related to the collision of microcontinent and island arc fragments during the Vendian–Ordovician evolution of this region. The Kokchetav massif is considered a mega-mélange zone (Dobretsov et al., 1995), in which rocks with different metamorphic history are mixed together (Shatsky et al., 1995).

To date, maruyamaite has been found in only two localities worldwide: the Kumdy-Kol microdiamond deposit (the type locality) (Shimizu and Ogasawara, 2005, 2013; Ota et al., 2008; Marschall et al., 2009; Lussier et al., 2016; Musiyachenko et al., 2020) and the Barchi-Kol area (Musiyachenko et al., 2021), both located within the western diamond-bearing Kumdy-Kol block in northern Kazakhstan (Dobretsov et al., 1995; Shatsky et al., 1995; Lavrova et al., 1999; Theunissen et al., 2000a, b; Korsakov et al., 2002). We collected samples of maruyamaite-bearing species and K-bearing tourmaline from the dumps of the underground gallery of the Kumdy-Kol microdiamond deposit and within the main gallery (Fig. 1) (Korsakov et al., 2023a, b, c). The tourmaline-bearing rocks are relatively fine grained and well foliated (Fig. 1, insert), although some samples may exhibit massive fabrics as well.

2 Materials, methods, and results

2.1 Starting material

Fragments of tourmaline crystals were mechanically extracted from the host rock by a stainless-steel clamp and selected under the microscope. More than 400 fragments with size of 100 to 500 µm were isolated and embedded in epoxy resin (Fig. 2).

2.2 SEM

Scanning electron microscopy (SEM) was performed on each sample with a Carl Zeiss EVO® 50 SEM available at the Department of Earth Sciences (Sapienza University of Rome), equipped with a W filament target and an SE Everhart–Thornley detector plus a quadrant backscatter detector (QBS) coupled with an energy-dispersive spectrometer (EDS) for qualitative elemental analysis. The resolution at 30 kV was 3.0 nm, and the acceleration voltage range was 0.2 to 30 kV, with a magnification power going from 5 to $10^6\times$. The presence of a possible zonation of major elements was checked with EDS spectra.

2.3 EMP

Portions of tourmaline with a homogeneous K content were mapped out using quantitative analysis of single spots with the electron microprobe (EMP). Chemical composition of the tourmaline samples was obtained using a wavelength-dispersive spectrometer (WDS mode) with a Cameca SX50 instrument at the Istituto di Geologia Ambientale e Geoingegneria (Rome, Italy), CNR, operating at an accelerating potential of 15 kV, with a 15 nA current and

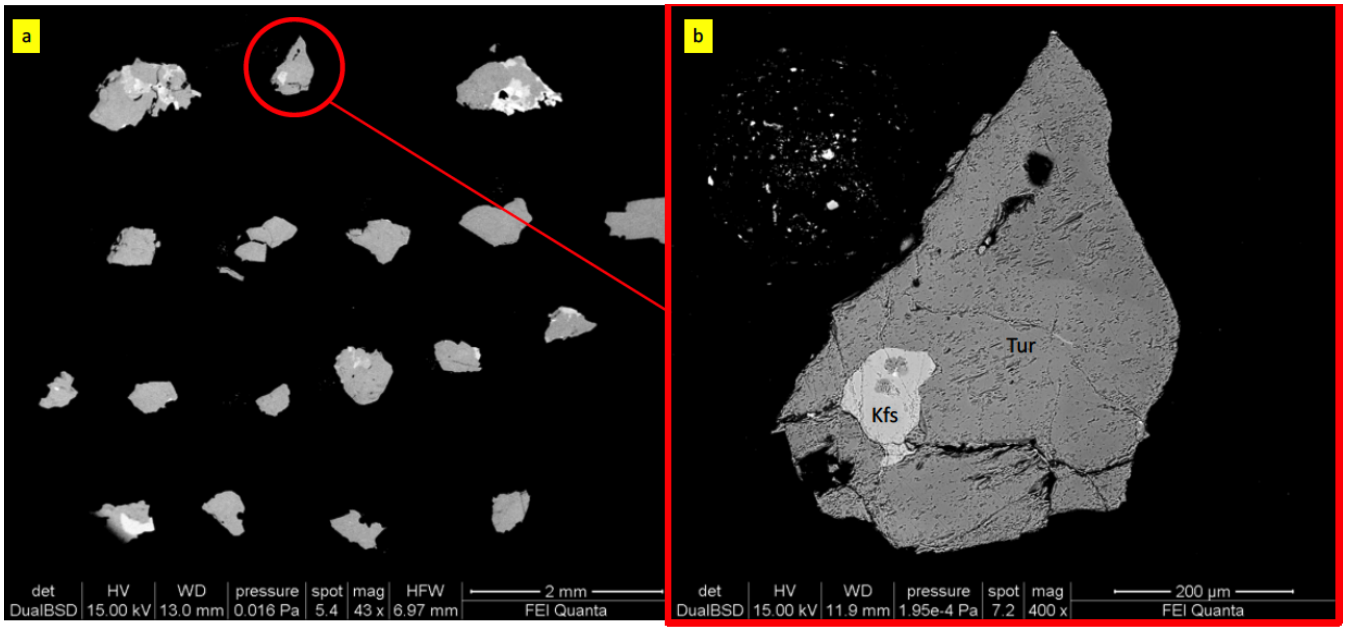

Figure 2. **(a)** Back-scattered electron image of some of the studied tourmaline crystal fragments embedded in epoxy; **(b)** detail of one of the fragments (2C2b) selected to extract the tourmaline portion; Tur: tourmaline; Kfs: K-feldspar.

a 10 µm beam diameter. Minerals and synthetic compounds were used as standards: wollastonite (Si, Ca), magnetite (Fe), rutile (Ti), corundum (Al), vanadinite (V), fluorphlogopite (F), periclase (Mg), jadeite (Na), orthoclase (K), sphalerite (Zn), rhodonite (Mn), metallic Cr, Ni and Cu. The PAP correction procedure for quantitative electron probe microanalysis was applied (Pouchou and Pichoir, 1991). Results are reported in Table 1. Vanadium, Cr, Ni and Cu were below their respective detection limits (0.03 wt %) in the studied samples.

2.4 SC-XRD

Nine crystal fragments with composition ranging from K-bearing oxy-dravite to maruyamaite were selected for single-crystal X-ray diffraction (SC-XRD) on a Bruker KAPPA APEX-II single-crystal diffractometer (Sapienza University of Rome, Earth Sciences Department), equipped with a charge-coupled device (CCD) area detector (6.2 cm × 6.2 cm active detection area, 512 × 512 pixels) and a graphite-crystal monochromator using Mo$K\alpha$ radiation from a fine-focus sealed X-ray tube. The sample-to-detector distance was 4 cm. A total of 3577 exposures (step = 0.2°, time/step = 20 s) covering the entire reciprocal sphere with a redundancy of ∼12 was collected. Final unit-cell parameters were refined using the Bruker AXS SAINT program on reflections with $I > 10\ \sigma_I$ in the range $6° < 2\theta < 75°$. The intensity data were processed and corrected for Lorentz, polarization and background effects using the APEX2 software program of Bruker AXS. The data were corrected for absorption using a multi-scan method (SADABS, Bruker AXS). The absorption correction led to an improvement in $R_{\rm int}$. No violation of $R3m$ symmetry was detected.

Structure refinement was done using the SHELXL-2013 program (Sheldrick, 2015). Starting coordinates were taken from Lussier et al. (2016). The variable parameters were the scale factor, extinction coefficient, atom coordinates, site-scattering values (for X, Y and Z sites) and atomic-displacement factors. As for the atomic model refinement and in accordance with the chemical analysis results (see below), the X site was modelled by setting the Na and K content to a variable content of atoms per formula unit (apfu) and by allowing the remainder of the site to refine as Ca. The Y site was modelled as Mg vs. Fe. The Z, T, B and anion sites were modelled, respectively, with Al, Si, B and O^{2-} scattering factors and with a fixed occupancy of 1, as refinement with unconstrained occupancies showed no significant deviations from this value. A final refinement was then performed by modelling the site occupancy of the O1 site with O and F fixed to the value obtained from the empirical formula (see below). The position of the H atom bonded to the oxygen at the O3 site in the structure was taken from the difference Fourier map and incorporated into the refinement model; the O3–H3 bond length was restrained (by the DFIX command) to be 0.97 Å, with the isotropic displacement parameter constrained to be equal to 1.2 times that obtained for the O3 site. There were no correlations greater than 0.7 between the parameters at the end of the refinement. Table 2 lists crystal data, data collection information and refinement details. The crystallographic information files showing all structural data have been deposited with the principal editor of the Euro-

Table 1. Chemical composition of the tourmaline crystal fragments studied.

Oxide/sample	24C2a	2C2b	14b	25b	32a	111a	92a	92b	92c
	avg of 5 spots	avg of 3 spots	avg of 3 spots	avg of 10 spots	avg of 3 spots	avg of 6 spots	avg of 11 spots	avg of 9 spots	avg of 5 spots
SiO_2 (wt.%)	36.12(0.29)	36.22(0.15)	36.49(0.38)	35.99(0.26)	36.97(0.21)	36.43(0.27)	35.91(0.24)	35.77(0.41)	36.16(0.49)
TiO_2	1.03(0.04)	1.05(0.05)	0.67(0.14)	0.66(0.10)	0.63(0.06)	0.61(0.05)	0.70(0.06)	0.70(0.07)	0.66(0.08)
B_2O_3[a]	10.46	10.49	10.57	10.51	10.71	10.55	10.45	10.46	10.52
Al_2O_3	31.96(0.25)	32.10(0.25)	32.13(0.59)	32.14(0.24)	32.05(0.10)	31.44(0.19)	31.96(0.33)	32.24(0.35)	32.02(0.44)
Cr_2O_3	0.03(0.03)	0.04(0.04)	0.04(0.03)	0.00	0.07(0.01)	0.07(0.02)	0.00	0.04(0.02)	0.00
V_2O_3	0.08(0.02)	0.06(0.01)	0.05(0.03)	0.04(0.02)	0.05(0.01)	0.04(0.02)	0.05(0.02)	0.04(0.02)	0.04(0.02)
FeO_{TOT}	2.82(0.18)	2.98(0.12)	2.84(0.46)	2.80(0.31)	2.45(0.13)	2.65(0.31)	2.92(0.13)	2.89(0.14)	2.80(0.29)
MgO	8.92(0.14)	8.80(0.09)	9.33(0.47)	9.32(0.46)	10.11(0.07)	9.95(0.27)	9.15(0.27)	9.07(0.09)	9.37(0.44)
CaO	1.12(0.05)	1.08(0.03)	1.64(0.23)	1.62(0.23)	1.99(0.08)	2.00(0.13)	1.48(0.20)	1.42(0.05)	1.61(0.29)
Na_2O	1.02(0.06)	1.07(0.04)	1.74(0.07)	1.53(0.22)	1.66(0.15)	1.43(0.68)	1.31(0.20)	1.16(0.05)	1.40(0.22)
K_2O	2.21(0.10)	2.12(0.05)	0.52(0.29)	0.88(0.53)	0.14(0.05)	0.30(0.07)	1.31(0.45)	1.65(0.07)	1.04(0.58)
F	0.16(0.07)	0.11(0.06)	0.33(0.18)	0.33(0.13)	0.57(0.07)	0.43(0.10)	0.40(0.13)	0.35(0.05)	0.34(0.05)
H_2O	2.84	2.88	2.87	2.89	2.90	2.95	2.83	2.86	2.89
$-O=F$	−0.07	−0.05	−0.14	−0.14	−0.24	−0.18	−0.17	−0.15	−0.15
FeO	2.54	2.68	2.56	2.52	2.21	2.39	2.63	2.60	2.52
Fe_2O_3[b]	0.31	0.33	0.32	0.31	0.27	0.29	0.32	0.32	0.31
Total	98.75	99.00	99.11	98.65	100.08	98.71	98.34	98.52	98.78
Atoms per formula unit (apfu) normalized to 31 anions									
Si	6.000	6.000	6.000	5.955	6.000	6.000	5.970	5.942	5.977
Ti	0.128	0.131	0.083	0.082	0.076	0.076	0.088	0.087	0.082
B	3.000	3.000	3.000	3.000	3.000	3.000	3.000	3.000	3.000
Al	6.257	6.267	6.227	6.266	6.129	6.103	6.261	6.313	6.237
Cr	0.004	0.006	0.005	0.000	0.008	0.009	0.000	0.005	0.000
V	0.011	0.008	0.006	0.006	0.006	0.005	0.007	0.005	0.005
Fe^{3+}	0.039	0.041	0.039	0.039	0.033	0.037	0.041	0.040	0.039
Fe^{2+}	0.353	0.372	0.351	0.349	0.299	0.329	0.366	0.361	0.348
Mg	2.209	2.174	2.288	2.298	2.447	2.443	2.268	2.246	2.308
Ca	0.200	0.191	0.289	0.287	0.346	0.353	0.263	0.252	0.285
Na	0.330	0.344	0.556	0.491	0.521	0.458	0.422	0.375	0.449
K	0.469	0.449	0.108	0.186	0.029	0.063	0.278	0.350	0.220
F	0.084	0.060	0.170	0.170	0.290	0.224	0.210	0.182	0.180
OH	3.152	3.179	3.144	3.194	3.138	3.245	3.139	3.166	3.182

Standard deviation is reported in brackets. Average: avg. [a] Calculated by stoichiometry, $(Y+Z+T+B)=18.000$ apfu. [b] The FeO / Fe_2O_3 ratio was assigned following Mössbauer spectroscopy data reported in Lussier et al. (2016).

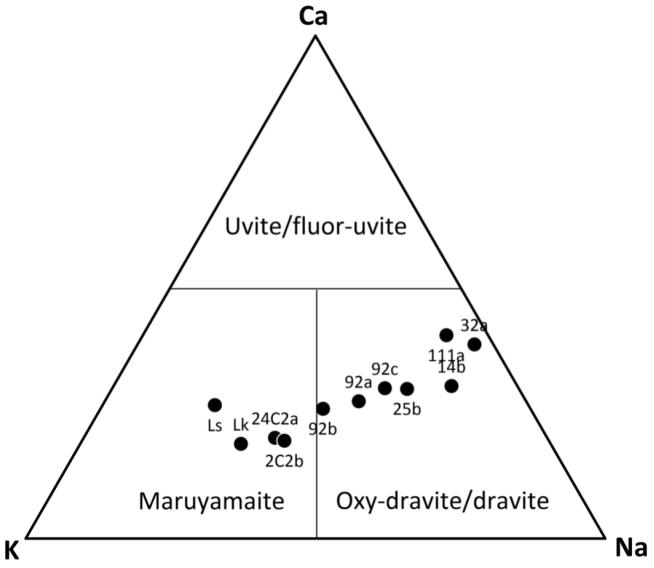

Figure 3. Ternary plot displaying the studied tourmalines on the basis of their *X* site population. Data from Lussier et al. (2016) and Likhacheva et al. (2019) are reported for comparison as "Ls" and "Lk", respectively.

pean Journal of Mineralogy and are available as a Supplement (Celata and Bosi, 2024).

2.5 Site populations

In agreement with the structure-refinement results, the boron content was assumed to be stoichiometric ($B^{3+} = 3.00$ apfu). The iron oxidation ratio was assigned on the basis of Mössbauer spectroscopic results reported in Lussier et al. (2016). In accordance with Pesquera et al. (2016), Li concentrations were considered insignificant as MgO > 2 wt % in the crystals studied. The (OH) content and the formula were then calculated by charge balance with the assumption $(T + Y + Z + B) = 18$ apfu and 31 anions.

The site populations at the *X*, *B*, *T*, O3 (≡ V) and O1 (≡ W) sites of the present crystals follow the standard site preference suggested for tourmaline (Henry et al., 2011). The Fe, Al and Mg site populations at the *Y* and *Z* sites were optimized according to the procedure of Bosi et al. (2017), as well as by fixing the minor Ti, V and Cr at *Y*. Calculated and observed site-scattering values at the different structural sites are listed in Table 3.

3 Discussion and conclusions

All the studied crystals fall in the maruyamaite–oxy-dravite/dravite compositional fields, as displayed in Fig. 3, with K contents ranging from 0.03 to 0.47 apfu (Table 1).

The *T* site can be considered to be practically fully occupied by Si, as shown by the limited variation of the mean bond distances < T–O > ranging from 1.618 to 1.620 Å (see

Table 2. Single-crystal X-ray diffraction data collected at room temperature for the tourmaline samples studied.

Sample	24C2a	2C2b	14b	25b	32a	111a	92a	92b	92c
Crystal size (mm)	0.16 × 0.20 × 0.20	0.24 × 0.21 × 0.07	0.12 × 0.10 × 0.02	0.28 × 0.28 × 0.20	0.16 × 0.12 × 0.09	0.20 × 0.14 × 0.12	0.16 × 0.14 × 0.08	0.24 × 0.21 × 0.16	0.16 × 0.12 × 0.04
a (Å)	15.92628(19)	15.9246(2)	15.9284(2)	15.92900(14)	15.93109(19)	15.9292(18)	15.9211(3)	15.9273(3)	15.9218(2)
c (Å)	7.22263(10)	7.2191O(10)	7.20010(10)	7.20700(10)	7.19726(9)	7.19972(10)	7.2149(2)	7.2067O(10)	7.21340(10)
V (Å^3)	1586.55(4)	1585.44(5)	1582.02(5)	1583.66(4)	1581.93(4)	1582.10(4)	1583.82(7)	1583.26(6)	1583.63(5)
Data collection range, 2θ (°)	6–75	6–75	6–73	6–73	6–73	6–73	6–73	6–73	5–73
Reciprocal space range *hkl*	$-27 \le h \le 26$ $-24 \le k \le 27$ $-12 \le l \le 11$	$-26 \le h \le 26$ $-26 \le k \le 27$ $-12 \le l \le 11$	$-25 \le h \le 26$ $-26 \le k \le 26$ $-8 \le l \le 11$	$-26 \le h \le 26$ $-26 \le k \le 26$ $-10 \le l \le 11$	$-26 \le h \le 26$ $-26 \le k \le 26$ $-12 \le l \le 12$	$-26 \le h \le 26$ $-26 \le k \le 26$ $-11 \le l \le 10$	$-26 \le h \le 26$ $-26 \le k \le 26$ $-10 \le l \le 8$	$-26 \le h \le 26$ $-26 \le k \le 22$ $-11 \le l \le 11$	$-26 \le h \le 26$ $-26 \le k \le 22$ $-10 \le l \le 10$
Number reflections	11 867	11 927	11 781	11 682	11 710	11 731	11 795	11 676	11 846
Unique reflections, R_{int} (%)	1770, 1.19	1902, 1.81	1698, 2.91	1679, 1.37	1850, 1.86	1813, 1.83	1636, 1.96	1804, 3.42	1718, 2.57
Redundancy	12	12	12	12	12	12	12	12	12
Extinction coefficient	0.00070(17)	0.00114(17)	0.00047(17)	0.00055(17)	0.00049(16)	0.00056(17)	0.00056(17)	0.0009(2)	0.00038(18)
Flack parameter	0.09(3)	0.10(4)	0.07(5)	0.08(4)	0.10(4)	0.10(4)	0.08(4)	0.07(4)	0.08(4)
w*R*2 (%)	3.21	3.26	3.79	3.27	3.35	3.33	3.33	3.62	3.60
*R*1 (%) all data	1.27	1.35	1.83	1.25	1.39	1.31	1.35	1.43	1.71
*R*1 (%) for $I > 2\sigma_I$	1.26	1.30	1.68	1.24	1.36	1.29	1.32	1.43	1.59
GooF	1.090	1.099	1.051	1.088	1.083	1.109	1.080	1.074	1.050

Table 3. Observed and calculated site-scattering values (epfu[a]) for the tourmaline samples studied.

Sample/site	*X*		*Y*		*Z*		*T*	
	obs	calc	obs	calc	obs[b]	calc	obs[b]	calc
24C2a	15.74(6)	16.53	43.01(13)	43.06	78.00	78.14	84.00	84.00
2C2b	15.40(6)	16.14	42.64(13)	42.84	78.00	78.68	84.00	84.00
14b	13.73(7)	13.95	42.34(13)	42.42	78.00	78.24	84.00	84.00
25b	14.26(6)	14.69	42.59(13)	42.60	78.00	78.03	84.00	83.95
32a	13.71(5)	13.20	42.26(13)	42.14	78.00	77.59	84.00	84.00
111a	13.99(6)	13.30	42.26(13)	42.23	78.00	77.90	84.00	84.00
92a	15.15(6)	15.19	42.64(13)	42.69	78.00	78.18	84.00	83.97
92b	14.19(7)	15.82	42.68(17)	42.74	78.00	78.12	84.00	83.94
92c	14.87(6)	14.82	43.35(13)	43.17	78.00	77.42	84.00	83.98

Calculated site-scattering values are from the crystal–chemical formula (Table 5). [a] epfu: electrons per formula unit. [b] Fixed in the final stages of refinement.

Table 4. Mean bond lengths of the tourmalines studied, bond-length (Δ_X) and volume (v_X) distortion indices, and discrepancy (δ, in valence units, vu) between the bond valence sum (BVS) and the mean formal charge at the *X* site.

Sample	$<X$–O$>$ (Å)	$<Y$–O$>$ (Å)	$<Z$–O$>$ (Å)	Δ_X (10^3)	v_X	δ (vu)
24C2a	2.687	2.009	1.933	0.981	0.1922	0.225
2C2b	2.684	2.009	1.932	1.118	0.1928	0.225
14b	2.666	2.017	1.930	2.102	0.1955	−0.084
25b	2.674	2.017	1.930	1.624	0.1946	−0.036
32a	2.665	2.017	1.929	2.135	0.1959	−0.186
111a	2.668	2.017	1.929	1.870	0.1953	−0.165
92a	2.681	2.009	1.932	1.184	0.1936	0.036
92b	2.673	2.014	1.931	1.567	0.1950	0.150
92c	2.677	2.011	1.932	1.326	0.1939	−0.016

Table 4), which correspond to the ideal distance $<{}^{T}\text{Si–O}> = 1.619(1)$ Å (e.g. Bosi and Lucchesi, 2007; Bačik and Fridrichová, 2021). The excess B (3.3 apfu) measured with SIMS by Marschall et al. (2009) in tourmaline samples from the Kumdy-Kol area was not evidenced by present structural refinement of single-crystal diffraction data. We doubt that B was deficient at the *B* site because the $<B$–O$>$ of all samples corresponds to the typically observed bond distance for B in planar triangular coordination in inorganic structures (Bosi and Lucchesi, 2007). Moreover, a B deficiency in tourmaline is stereochemically unlikely (Hawthorne, 1996).

From a crystal–chemical viewpoint, the studied samples can be described as Fe^{2+}-rich maruyamaite (samples 24C2a and 2C2b) and Fe^{2+}- and F-rich oxy-dravite (see Table 5). Our samples are also relatively rich in Ca (Fig. 3), which is inversely correlated to K ($r^2 = 0.93$) and only roughly directly correlated to Na ($r^2 = 0.62$). Calcium represents the minor fluor-uvite component of the samples, similarly to observations by Musiyachenko et al. (2020). The relation among K, Na and Ca may be approximated as K = (Na + Ca), with the Na : Ca ratio in the range (1.5–2) : 1 (the limited extent of vacancy at the *X* site was not considered here).

The compositional variability of our samples can be ideally expressed as a sequence of substitutions going from maruyamaite to oxy-dravite, dravite and fluor-uvite (or vice versa) (Fig. 4). Leaving out the fluor-uvitic component, the substitutions that lead from maruyamaite to oxy-dravite to dravite are (1) $^{X}\text{K} + \text{Al}_{\text{TOT}} + {}^{O1}\text{O} \leftrightarrow {}^{X}\text{Na} + \text{Mg}_{\text{TOT}} + {}^{O1}\text{O}$ and (2) $^{X}\text{Na} + \text{Mg}_{\text{TOT}} + {}^{O1}\text{O} \leftrightarrow {}^{X}\text{Na} + \text{Mg}_{\text{TOT}} + {}^{O1}\text{OH}$, respectively. Conversely, leaving out the maruyamaitic component, the substitutions that lead from oxy-dravite to dravite to fluor-uvite are (1) $^{X}\text{Na} + \text{Mg}_{\text{TOT}} + {}^{O1}\text{O} \leftrightarrow {}^{X}\text{Na} + \text{Mg}_{\text{TOT}} + {}^{O1}\text{OH}$ and (2) $^{X}\text{Na} + \text{Mg}_{\text{TOT}} + {}^{O1}\text{OH} \leftrightarrow {}^{X}\text{Ca} + \text{Mg}_{\text{TOT}} + {}^{O1}\text{F}$, respectively. In our samples, the fluor-uvitic component increases towards oxy-dravite and dravite.

In all samples, the *Z* site has a constant site population with the Al : Mg ratio $\approx 5 : 1$, which is supported by a range of $<Z$–O$>$ limited to 1.929 to 1.933 Å (Table 4). The global distortion of ZO_6 was calculated as the quadratic elongation $<\lambda_Z>$ (Robinson et al., 1971), which shows an increase with the structural expansion and thus with the maruyamaitic component (Fig. 5), consistent with the correlation reported by Bosi and Lucchesi (2007).

https://doi.org/10.5194/ejm-36-797-2024

Table 5. Crystal–chemical formulas of the tourmaline crystal fragments studied and their classification.

Sample	Crystal–chemical formula
24C2a (maruyamaite)	$^{X}(K_{0.47}Na_{0.33}Ca_{0.20})_{\Sigma 1.00}\,^{Y}(Mg_{1.28}Al_{1.27}Fe^{2+}_{0.31}Ti_{0.13}V_{0.01})_{\Sigma 3.00}\,^{Z}(Al_{4.99}Mg_{0.93}Fe^{2+}_{0.04}Fe^{3+}_{0.04})_{\Sigma 6.00}\,^{T}Si_6O_{18}(BO_3)_3\,^{O3}(OH)^{O1}_3[(OH)_{0.15}F_{0.08}O_{0.77}]_{\Sigma 1.00}$
2C2b (maruyamaite)	$^{X}(K_{0.45}Na_{0.34}Ca_{0.19}\square_{0.02})_{\Sigma 1.00}\,^{Y}(Mg_{1.31}Al_{1.25}Fe^{2+}_{0.29}Ti_{0.25}V_{0.01}Cr_{0.01})_{\Sigma 3.00}\,^{Z}(Al_{5.01}Mg_{0.87}Fe^{2+}_{0.08}Fe^{3+}_{0.04})_{\Sigma 6.00}\,^{T}Si_6O_{18}(BO_3)_3\,^{O3}(OH)^{O1}_3[(OH)_{0.18}F_{0.06}O_{0.76}]_{\Sigma 1.00}$
14b (oxy-dravite)	$^{X}(K_{0.11}Na_{0.56}Ca_{0.29}\square_{0.05})_{\Sigma 1.00}\,^{Y}(Mg_{1.44}Al_{1.15}Fe^{2+}_{0.31}Ti_{0.08}V_{0.01}Cr_{0.01})_{\Sigma 3.00}\,^{Z}(Al_{5.07}Mg_{0.84}Fe^{2+}_{0.04}Fe^{3+}_{0.04})_{\Sigma 6.00}\,^{T}Si_6O_{18}(BO_3)_3\,^{O3}(OH)^{O1}_3[(OH)_{0.14}F_{0.17}O_{0.69}]_{\Sigma 1.00}$
25b (oxy-dravite)	$^{X}(K_{0.19}Na_{0.49}Ca_{0.29}\square_{0.04})_{\Sigma 1.00}\,^{Y}(Mg_{1.43}Al_{1.15}Fe^{2+}_{0.32}Ti_{0.08}V_{0.01})_{\Sigma 3.00}\,^{Z}(Al_{5.07}Mg_{0.86}Fe^{2+}_{0.03}Fe^{3+}_{0.04})_{\Sigma 6.00}[^{T}(Si_{5.95}Al_{0.05})_{\Sigma 6.00}O_{18}]\,(BO_3)^{O3}_3(OH)^{O1}_3[(OH)_{0.19}F_{0.17}O_{0.64}]_{\Sigma 1.00}$
32a (oxy-dravite)	$^{X}(K_{0.03}Na_{0.52}Ca_{0.35}\square_{0.10})_{\Sigma 1.00}\,^{Y}(Mg_{1.51}Al_{1.10}Fe^{2+}_{0.29}Ti_{0.08}V_{0.01}Cr_{0.01})_{\Sigma 3.00}\,^{Z}(Al_{5.02}Mg_{0.93}Fe^{2+}_{0.01}Fe^{3+}_{0.03})_{\Sigma 6.00}\,^{T}Si_6O_{18}(BO_3)_3\,^{O3}(OH)^{O1}_3[(OH)_{0.14}F_{0.29}O_{0.57}]_{\Sigma 1.00}$
111a (oxy-dravite)	$^{X}(K_{0.06}Na_{0.46}Ca_{0.35}\square_{0.13})_{\Sigma 1.00}\,^{Y}(Mg_{1.51}Al_{1.10}Fe^{2+}_{0.30}Ti_{0.08}V_{0.01}Cr_{0.01})_{\Sigma 3.00}\,^{Z}(Al_{5.00}Mg_{0.93}Fe^{2+}_{0.03}Fe^{3+}_{0.04})_{\Sigma 6.00}\,^{T}Si_6O_{18}(BO_3)_3\,^{O3}(OH)^{O1}_3[(OH)_{0.25}F_{0.22}O_{0.53}]_{\Sigma 1.00}$
92a (oxy-dravite)	$^{X}(K_{0.28}Na_{0.42}Ca_{0.26}\square_{0.04})_{\Sigma 1.00}\,^{Y}(Mg_{1.32}Al_{1.27}Fe^{2+}_{0.32}Ti_{0.09}V_{0.01})_{\Sigma 3.00}\,^{Z}(Al_{4.96}Mg_{0.95}Fe^{2+}_{0.05}Fe^{3+}_{0.04})_{\Sigma 6.00}[^{T}(Si_{5.97}Al_{0.03})_{\Sigma 6.00}O_{18}]\,(BO_3)^{O3}_3(OH)^{O1}_3[(OH)_{0.14}F_{0.21}O_{0.65}]_{\Sigma 1.00}$
92b (oxy-dravite)	$^{X}(K_{0.35}Na_{0.38}Ca_{0.25}\square_{0.02})_{\Sigma 1.00}\,^{Y}(Mg_{1.38}Al_{1.20}Fe^{2+}_{0.33}Ti_{0.09}V_{0.01}Cr_{0.01})_{\Sigma 3.00}\,^{Z}(Al_{5.06}Mg_{0.87}Fe^{2+}_{0.04}Fe^{3+}_{0.04})_{\Sigma 6.00}[^{T}(Si_{5.94}Al_{0.06})_{\Sigma 6.00}O_{18}]\,(BO_3)_3\,^{O3}(OH)^{O1}_3[(OH)_{0.17}F_{0.18}O_{0.65}]_{\Sigma 1.00}$
92c (oxy-dravite)	$^{X}(K_{0.22}Na_{0.45}Ca_{0.29}\square_{0.05})_{\Sigma 1.00}\,^{Y}(Mg_{1.31}Al_{1.25}Fe^{2+}_{0.35}Ti_{0.08}V_{0.01})_{\Sigma 3.00}\,^{Z}(Al_{4.97}Mg_{1.00}Fe^{3+}_{0.03})_{\Sigma 6.00}[^{T}(Si_{5.98}Al_{0.02})_{\Sigma 6.00}\,O_{18}]\,(BO_3)_3\,^{O3}(OH)^{O1}_3[(OH)_{0.18}F_{0.18}O_{0.64}]_{\Sigma 1.00}$

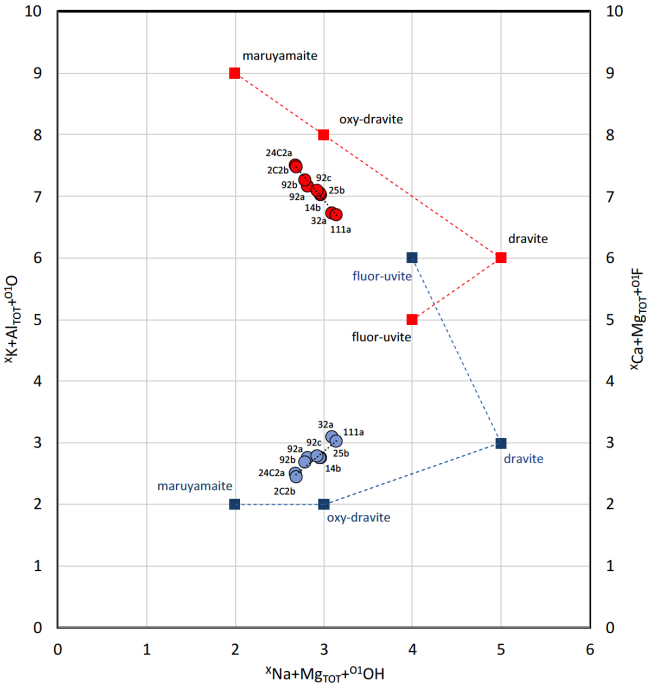

Figure 4. Substitutions that ideally tie maruyamaite to oxy-dravite, dravite and fluor-uvite. Data are reported in atoms per formula unit (apfu). Total Al and total Mg apfu from both the Y and Z sites were considered to avoid any issue due to cation disorder. Labelling of samples as in Fig. 3. Data from Berryman et al. (2016) are not shown because their maruyamaite (actually potassium-dravite) was synthesized under conditions not representing natural environments. Red dots refer to the left y axis and represent the studied compositional series, the trend of which is ideally shown by the dashed red line that leads from maruyamaite to oxy-dravite to dravite through the following substitutions: (1) $^{X}K + Al_{TOT} + ^{O1}O \leftrightarrow {}^{X}Na + Mg_{TOT} + {}^{O1}O$ and (2) $^{X}Na + Mg_{TOT} + {}^{O1}O \leftrightarrow {}^{X}Na + Mg_{TOT} + {}^{O1}OH$. Blue dots refer to the right y axis and represent the same studied samples, the trend of which is shown by the dashed blue line that leads from oxy-dravite to dravite to fluor-uvite through the following substitutions: (1) $^{X}Na + Mg_{TOT} + {}^{O1}O \leftrightarrow {}^{X}Na + Mg_{TOT} + {}^{O1}OH$ and (2) $^{X}Na + Mg_{TOT} + {}^{O1}OH \leftrightarrow {}^{X}Ca + Mg_{TOT} + {}^{O1}F$.

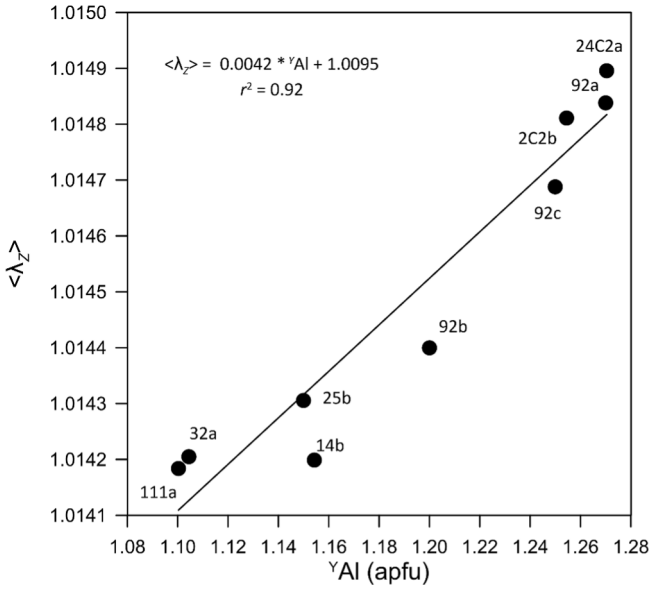

Figure 5. Relation between the ZO_6 quadratic elongation $< \lambda_Z >$ (Robinson et al., 1971) and the Al content at the Y site.

A more pronounced chemical variation is instead observed at the Y site, which is dominated by Mg ranging from 1.28 to 1.51 apfu, followed by Al 1.10–1.27 apfu, Fe^{2+} 0.29–0.33 apfu, and Ti up to 0.25 apfu. The variation of a small cation like Al significantly influences the $< Y$–O $>$ values, as shown in Fig. 6a. It is worth noting that when ^{Y}Al is 3 apfu, $< Y$–O $>$ equals 1.906 Å, which aligns perfectly with the ionic radii of Bosi and Lucchesi (2007).

The largest chemical variation is observed at the X site, which is characterized by the substitution of K for Na and minor Ca (Table 5). The incorporation of K at the X site causes the enlargement of the XO_9 polyhedron, as demonstrated by the linear increase in $< X$–O $>$ from 2.665 to 2.687 Å with the K content (Fig. 6b). The sample synthesized by Berryman et al. (2016) lies off this trend, perhaps because their sample, actually a potassium-dravite, has a significant proportion of vacancies at the X site (0.3 apfu) that may further enlarge $< X$–O $>$, according to the bond lengths for the X site calculated by Bačík and Fridrichová (2021). The enlargement of XO_9 due to an increase in the K content determines a parallel increase in the unit-cell c parameter from 7.197 to 7.223 Å (Fig. 6c) and the unit-cell volume from 1582 to 1586 Å^3 (Fig. 6d). Conversely, no correlation between the K content and the a parameter was observed.

The uptake of K along the oxy-dravite–maruyamaite series is related to the structural distortion of the XO_9 polyhedron. Distortion indices for XO_9 can be calculated in terms of bond-length distortion, using the formula $\Delta_X = \frac{1}{9}\sum_1^9[(d_i - d_m/d_m]^2$ (Ertl et al., 2002), or polyhedral volume distortion, using the formula $\nu_X = (V_i - V_p)/V_i$, where V_i and V_p are ideal and observed polyhedral volume (Balić-Žunić and Makovicky, 1996; Balić-Žunić, 2007). The resulting values are listed in Table 4, and they are positively correlated ($r^2 = 0.92$) along the oxy-dravite–maruyamaite series. Figure 7 shows the inverse correlation between the ν_X values, representing the volume XO_9 distortion with the K content. The average value of ν_X (0.194 ± 0.001) appears to be intermediate when compared to the smallest one calculated for povondraite (0.188 ± 0.001 from five samples reported in Bosi et al., 2023), to that for ^{Y}Al-rich oxy-tourmaline (0.206 from sample RED-T4 in Ertl et al., 2005) and to the largest one observed for buergerite (0.215, Barton, 1969). Disregarding buergerite, ν_X decreases with increasing cell volume: 1526.9 Å^3 for sample RED-T4, 1586.6 Å^3 for maruyamaite (sample 24C2a, present study) and 1705.2 Å^3 for povondraite (sample pov5, Bosi et al., 2023).

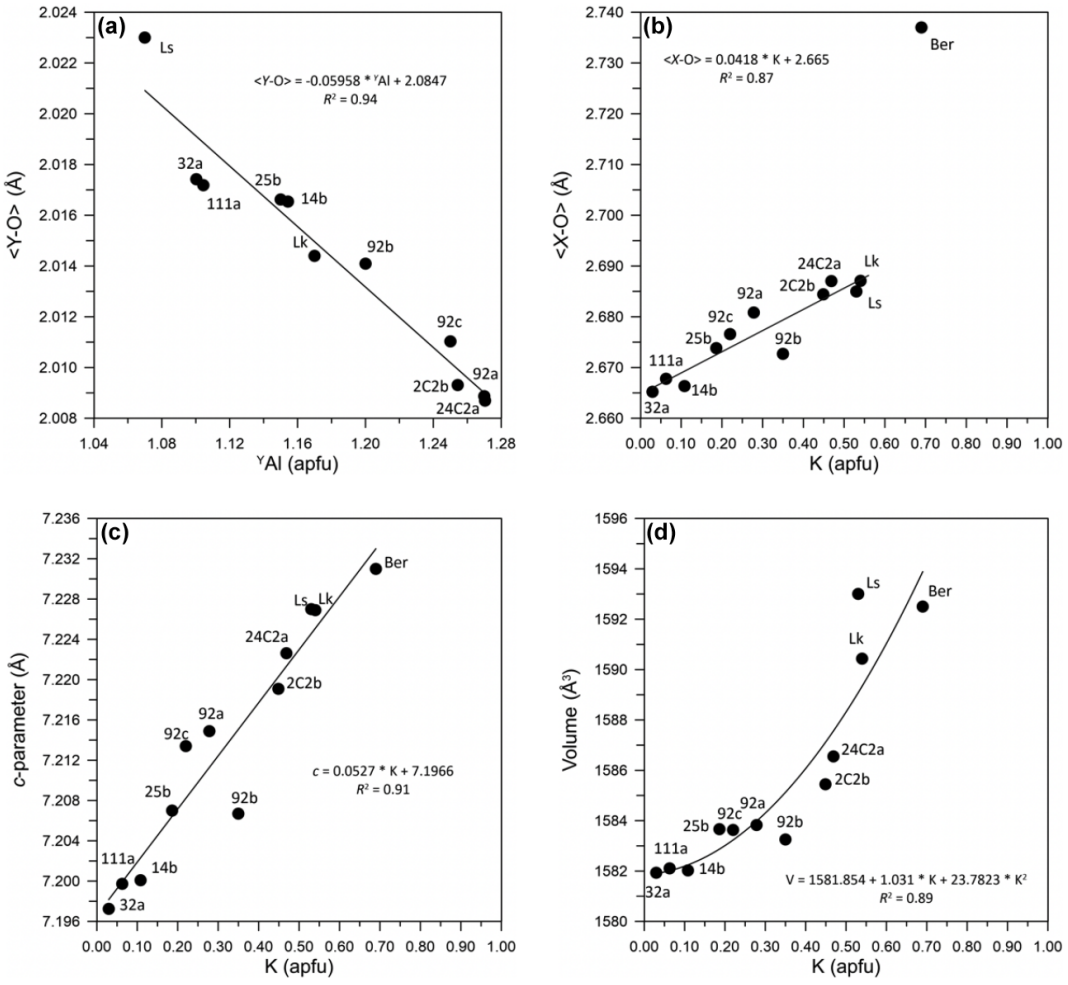

Figure 6. Structural vs. compositional parameters for the studied tourmaline samples. **(a)** Dependence of $< Y\text{–O} >$ mean bond length on the Al content at the Y site. Data from Lussier et al. (2016), Berryman et al. (2016) and Likhacheva et al. (2019) are reported for comparison as "Ls", "Ber" and "Lk", respectively. **(b)** Dependence of $< X\text{–O} >$ mean bond length on the K content at the X site. **(c)** Dependence of cell parameter c on the K content at the X site. **(d)** Dependence of cell volume V on the K content at the X site. Symbol size is larger than the experimental error.

At the X site, the distribution of local discrepancy (δ) between the bond valence sum (BVS, calculated from parameters of Brown and Altermatt, 1985) and the mean formal charge reveals an XO_9 compression (overbonding) for $K > 0.21$ apfu, which is towards maruyamaite, and an XO_9 extension (underbonding) for $K < 0.21$ apfu, which is towards oxy-dravite (Table 4 and Fig. 8). It is worth mentioning that tourmalines with the X site completely occupied by Na, such as oxy-chromium-dravite (Bosi et al., 2012), exhibit δ values of approximately -0.2 vu (underbonding). This finding demonstrates that the tourmaline structure can effectively accommodate the excessive overbonding of the X site, as occurs for dravite at high-pressure (HP) conditions (O'Bannon et al., 2018).

The issue of the structural stability of maruyamaite, as well as the influence of genetic conditions (pressure vs. chemical environment) on K uptake in the tourmaline structure, is not completely disentangled yet. Berryman et al. (2015) demonstrated that K concentration in the crystallization fluid (and absence of the competitor element Na) is the essential condition to have maruyamaite. From the same experimental work, it turned out that pressure is as important as fluid composition to squeeze the relatively large K cation into the tighter X cavity (up to 4 GPa to obtain 0.583 apfu K). This is particularly true where the tourmaline Z site is dominated by Al (e.g. maruyamaite), which gives a smaller 3D framework made of ZO_6 polyhedra. Conversely, in K-dominant tourmalines with povondraite composition occurring in meta-evaporite environments (Začek et al., 1998), the accommodation of K at low pressure is favoured by a larger 3D framework made of $^{Z}Fe^{3+}O_6$ polyhedra (Bačík et al., 2008; Hovis et al., 2023). Compared to the K-dominant analogues with povondraite-

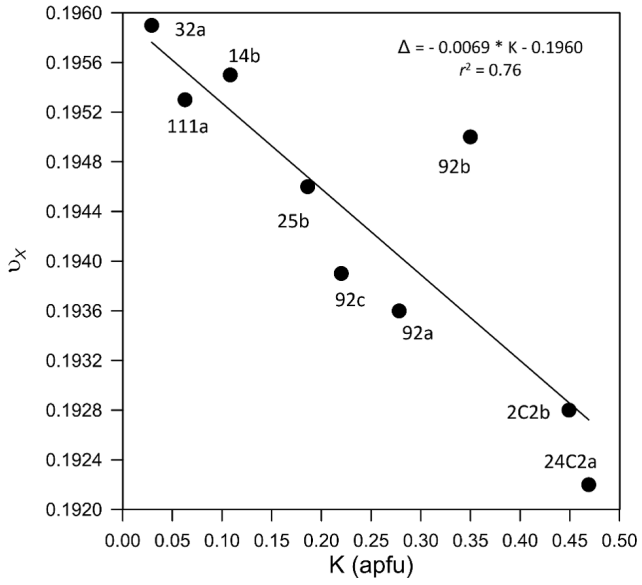

Figure 7. Correlation between the polyhedral XO_9 volume distortion index (υ_X, as defined by Balić-Žunić and Makovicky, 1996) and the K content at the *X* site.

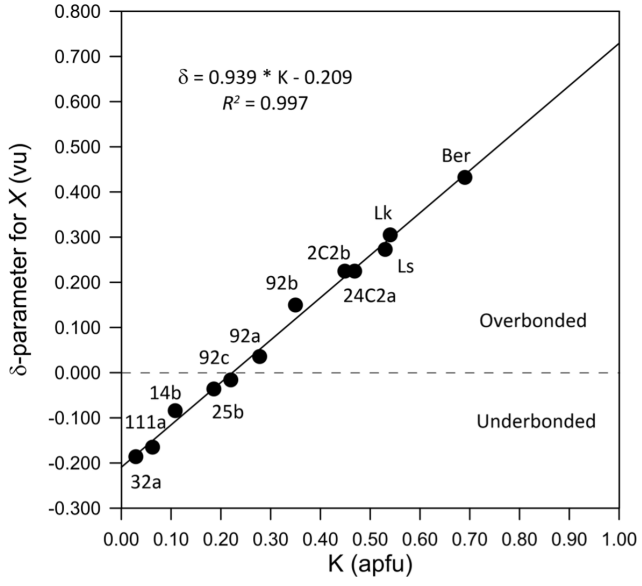

Figure 8. Plot of δ for the *X* site vs. the K content for the nine investigated tourmaline crystals. See text for explanation.

type framework, maruyamaite should hence only be stable in ultrapotassic environments and relatively high pressure conditions.

In other minerals stable at HP conditions, for example pyroxenes, the ionic radius of K was considered too large to fit the relatively small $M2O_8$ polyhedron without leading to catastrophic effects on the mineral stability, and K accommodation in the structure was commonly unaccepted up to the 1980s (e.g. Papike, 1980). Multiple findings of K-rich pyroxene in garnet–clinopyroxene–carbonate rocks of the Kokchetav UHP complex (Sobolev and Shatsky, 1990), K-rich clinopyroxene inclusions in kimberlitic diamonds (e.g. Sobolev et al., 1998; Stachel et al., 2000; Kaminsky et al., 2000; Pokhilenko et al., 2004) and K-rich pyroxenes synthesized at UHP conditions (discussed in Safonov et al., 2011) revealed that clinopyroxene better accommodates K at the *M2* site, with pressure increasing up to a maximum of 7–8 GPa, since the relatively large K atom is sufficiently soft to shrink and fit into the more comparatively small $M2O_8$ polyhedron at high pressure. In contrast, in layered K-minerals such as the white mica phengite that are commonly reported in HP–UHP units (e.g. Gouzu et al., 2016), K is easily accommodated in the crystal structure as an interlayer cation even at room pressure due to the large volume of the cavity where it is hosted.

The origin of maruyamaite and K-bearing tourmalines from the Kumdy-Kol microdiamond deposit is under debate with two primary models proposed: (i) metamorphic (Shimizu and Ogasawara, 2005, 2013; Ota et al., 2008) and (ii) metasomatic (Lavrova et al., 1999; Korsakov et al., 2009; Marschall et al., 2009). The discovery of diamond inclusions within the ultrapotassic cores of the tourmalines supports the UHP metamorphic origin of maruyamaite (Shimizu and Ogasawara, 2005, 2013; Ota et al., 2008). Additionally, the stepwise decrease in the K content from the core to the rim of the crystals is interpreted as indicative of these zones growing during the exhumation of diamond-bearing rocks (Shimizu and Ogasawara, 2005, 2013; Ota et al., 2008). However, an alternative explanation arises from the lack of other UHP mineral indicators (except for diamond), the unusual isotopic composition of B in K-bearing tourmaline, and the high abundances of tourmalines in the rock samples (approximately 20 vol %). These factors suggest that the crystallization of these tourmalines is more likely related to metasomatic processes (Korsakov et al., 2009; Marschall et al., 2009).

Argon–argon (Ar–Ar) dating of K-bearing tourmalines (with $K_2O \sim 1.6$ wt %) and muscovite from a sample revealed ages of 491.5 ± 4.9 and 492 ± 4.8 Ma, respectively, supporting the metasomatic origin of these tourmalines at mid-crustal levels (Korsakov et al., 2009). However, these K-bearing tourmalines could not be classified as maruyamaite, and the dating results were questioned (Shimizu and Ogasawara, 2013). More recently, Ar–Ar dating was performed on three additional tourmaline samples (Korsakov et al., 2023a). Two of these samples had maruyamaite composition, while the third, with a K_2O content not exceeding 1.8 wt %, did not qualify as maruyamaite but contained diamond inclusions. All these tourmalines yielded well-defined Ar–Ar ages of 502.3 ± 8.0, 502.2 ± 8.0, 506.0 ± 8.0 Ma, which are statistically identical within the stated error margin. This indicates no correlation between Ar–Ar ages and different K contents in tourmaline crystals. Moreover, these ages are significantly younger than the 530 Ma age determined for the

peak of UHP metamorphism by various methods (Claoue-Long et al., 1991; Shatsky et al., 1999; Hermann et al., 2001, 2006b; Katayama et al., 2001; Stepanov et al., 2016). Consequently, it is likely that the crystallization of maruyamaite and other K-bearing tourmalines from the Kumdy-Kol microdiamond deposit occurred significantly later than the peak metamorphism.

K-feldspar inclusions commonly found in tourmaline crystals with variable K content considered in this study (see Fig. 2b) represent a valuable tool for constraining the upper stability limit of tourmaline. Experimental studies (e.g. Seki and Kennedy, 1964; Yagi et al., 1994; Urakawa et al., 1994) have shown that K-feldspar (sanidine) breaks down at 1000–1200 °C and 6–7 GPa under dry conditions. However, Hermann and Green (2001) observed that K-feldspar was not stable above 1050 °C and 3.5 GPa in the K_2O–CaO–MgO–Al_2O_3–SiO_2–H_2O system. This supports our hypothesis that K-tourmaline from the Kokchetav Massif may have crystallized under HP conditions, with an upper limit ranging from 3.5 to 7 GPa during retrograde metamorphism, which occurred after the UHP metamorphic peak.

Data availability. The full data set is available on Zenodo at https://doi.org/10.5281/zenodo.13383156 (Celata and Bosi, 2024).

Author contributions. The starting material was provided by KAM and MVK; the characterization was performed by BC, FB and GBA; and the data validation and original draft preparation were carried out by the whole research team.

Competing interests. The contact author has declared that none of the authors has any competing interests.

Disclaimer. Publisher's note: Copernicus Publications remains neutral with regard to jurisdictional claims made in the text, published maps, institutional affiliations, or any other geographical representation in this paper. While Copernicus Publications makes every effort to include appropriate place names, the final responsibility lies with the authors.

Acknowledgements. We sincerely thank the reviewers Peter Bacik and Andreas Ertl for their valuable suggestions, as well as the associate editor Edward Grew for the constructive discussion and thorough revision of the paper.

Financial support. This research was supported by Sapienza University of Rome (Progetto Università 2022) and PRIN 2020, Ministero Università e Ricerca (HYDROX – HYDRous- vs. OXo-components in minerals: adding new pieces to the Earth's H_2O cycle puzzle), funding for Ferdinando Bosi and Giovanni B. Andreozzi. The state assignment of IGM SB RAS (122041400241-5) supported Andrey V. Korsakov and Kira A. Musiyachenko. Publisher's note: the article processing charges for this publication were not paid by a Russian or Belarusian institution.

Review statement. This paper was edited by Edward Grew and reviewed by Andreas Ertl and Peter Bacik.

References

Bačík, P. and Fridrichová, J.: Cation partitioning among crystallographic sites based on bond-length constraints in tourmaline-supergroup minerals, Am. Mineral., 106, 851–861, 2021.

Bačík, P., Uher, P., Sykora, M., and Lipka, J.: Low-Al tourmalines of the schorl – dravite – povondraite series in redeposited tourmalinites from the Western Carpathians, Slovakia, Canad. Mineral., 46, 1117–1129, 2008.

Balić-Žunić, T.: Use of three-dimensional parameters in the analysis of crystal structures under compression, in: Pressure-Induced Phase Transitions, edited by: Grzechnik, A., Transworld Research Network, Trivandrum, Kerela, India, 157–184, 2007.

Balić-Žunić, T. and Makovicky, E.: Determination of the Centroid or "the Best Centre" of a Coordination Polyhedron, Acta Crystallogr. B, 52, 78–81, 1996.

Barton Jr., R.: Refinement of the crystal structure of buergerite and the absolute orientation of tourmalines, Acta Crystallogr. B, 25, 1524–1533, 1969.

Berryman, E. J., Wunder, B., and Rhede, D.: Synthesis of K-dominant tourmaline, Am. Mineral. 99, 539–542, 2014.

Berryman, E. J., Wunder, B., Wirth, R., Rhede, D., Schettler, G., Franz, G., and Heinrich, W.: An experimental study on K and Na incorporation in dravitic tourmaline and insight into the origin of diamondiferous tourmaline from the Kokchetav Massif, Kazakhstan, Contrib. Mineral. Petrol., 169, 1–16, 2015.

Berryman, E. J., Wunder, B., Ertl, A., Koch-Müller, M., Rhede, D., Scheidi, K., Giester, G., and Heinrich, W.: Influence of the X-site composition on tourmaline's crystal structure: investigation of synthetic K-dravite, dravite, oxy-uvite, and magnesio-foitite using SREF and Raman spectroscopy, Phys. Chem. Miner., 43, 83–102, 2016.

Bishop, F. C., Smith, J. V., and Dawson, J. B.: Na, K, P and Ti in garnet, pyroxene and olivine from peridotite and eclogite xenoliths from African kimberlites, Lithos, 11, 155–173, 1978.

Bosi, F.: Tourmaline crystal chemistry, Am. Mineral., 103, 298–306, 2018.

Bosi, F. and Lucchesi, S.: Crystal chemical relationships in the tourmaline group: Structural constraints on chemical variability, Am. Mineral., 92, 1054–1063, 2007.

Bosi, F., Reznitskii, L., and Skogby, H.: Oxy-chromium-dravite, $NaCr_3(Cr_4Mg_2)(Si_6O_{18})(BO_3)_3(OH)_3O$, a new mineral species of the tourmaline supergroup, Am. Mineral., 97, 2024–2030, 2012.

Bosi. F., Reznitskii, L., Hålenius, U., and Skogby, H.: Crystal chemistry of Al-V-Cr oxy-tourmalines from Sludyanka complex, Lake Baikal, Russia, Eur. J. Mineral., 29, 457–472, https://doi.org/10.1127/ejm/2017/0029-2617, 2017.

Bosi, F., Skogby, H., and Hovis, G. L.: Crystal chemistry of povondraite by single-crystal XRD, EMPA, Mössbauer spectroscopy and FTIR, Mineral. Mag., 87, 178–185, 2023.

Brown, I. D. and Altermatt, D.: Bond-valence parameters obtained from a systematic analysis of the Inorganic Crystal Structure Database, Acta Crystallogr. B, 41, 244–247, 1985.

Celata, B. and Bosi, F.: Crystallographic Information File on K-tourmaline from Kazakhstan, Zenodo [data set], https://doi.org/10.5281/zenodo.13383156, 2024.

Claoue-Long, J. C., Sobolev, N. V., Shatsky, V. S., and Sobolev, A. V.: Zircon response to diamond-pressure metamorphism in the Kokchetav massif, USSR, Geology, 19, 710–713, 1991.

Dobretsov, N. L., Sobolev, N. V., Shatsky, V. S., Coleman, R. G., and Ernst, W. G.: Geotectonic evolution of diamondiferous paragneisses of the Kokchetav complex, Northern Kazakhstan - the geologic enigma of ultrahigh-pressure crustal rocks within Phanerozoic foldbelt, Isl. Arc., 4, 267–279, 1995.

Dutrow, B. L. and Henry, D. J.: Tourmaline; a geologic DVD, Elements, 7, 301–306, 2011.

Erlank, A. J. and Kushiro, I.: Potassium contents of synthetic pyroxenes at high temperatures and pressures, Carnegie Inst. Wash yearbook, 68, 439–442, 1970.

Ertl, A., Hughes, J. M., Pertlik, F., Foit Jr., F. F., Wright, S. E., Brandstätter, F., and Marler, B.: Polyhedron distortions in tourmaline, Canad. Mineral., 40, 153–163, 2002.

Ertl, A., Rossman, G.R., Hughes, J.M, Prowatke, S., and Ludwig, T.: Mn-bearing "oxy-rossmanite" with tetrahedrally coordinated Al and B from Austria: Structure, chemistry, and infrared and optical spectroscopic study, Am. Mineral., 90, 481–487, 2005.

Ertl, A., Marschall, H. R., Giester, G., Henry, D. J., Schertl, H. P., Ntaflos, T., Luvizzotto, G. L., Nasdala, L., and Tillmanns, E.: Metamorphic ultrahigh-pressure tourmaline: Structure, chemistry, and correlations to $P-T$ conditions, Am. Mineral., 95, 1, 1–10, 2010.

Gouzu, C., Yagi, K., Xhuan Thanh, N., Itaya, T., and Compagnoni, R.: White mica K–Ar geochronology of HP–UHP units in the Lago di Cignana area, western Alps, Italy: Tectonic implications for exhumation, Lithos, 248–251, 109–118, 2016.

Grew, E. S., Krivovichev, S. V., Hazen, R. M., and Hystad, G.: Evolution of structural complexity in Boron minerals, Canad. Mineral., 54, 125–143, 2016.

Grice, J. D., Ercit, T. S., and Hawthorne, F. C.: Povondraite, a redefinition of the tourmaline ferridravite, Am. Mineral., 78, 433–436, 1993.

Hawthorne, F. C.: Structural mechanisms for light-element variations in tourmaline, Canad. Mineral., 34, 123–132, 1996.

Harlow, G. E. and Davies, R.: Status report on stability of K-rich phases at mantle conditions, Lithos, 77, 647–653, 2004.

Henry, D. J. and Dutrow, B. L.: Tourmaline in a low grade clastic metasedimentary rock: an example of the petrogenetic potential of tourmaline, Contrib. Mineral. Petrol., 112, 203–218, 1992.

Henry, D. J., Novák, M., Hawthorne, F. C., Ertl, A., Dutrow, B. L., Uher, P., and Pezzotta, F.: Nomenclature of the tourmaline-supergroup minerals, Am. Mineral., 96, 895–913, 2011.

Hermann, J. and Green, D. H.: Experimental constraints on high pressure melting in subducted crust, Earth Planet. Sc. Lett., 188, 149–186, 2001.

Hermann, J., Rubatto, D., Korsakov, A., and Shatsky, V. S.: Multiple zircon growth during fast exhumation of diamondiferous, deeply subducted continental crust (Kokchetav massif, Kazakhstan), Contrib. Mineral. Petrol., 141, 66–82, 2001.

Hermann, J., Spandler, C., Hack, A., and Korsakov, A. V.: Aqueous fluids and hydrous melts in high-pressure and ultra-high pressure rocks: Implications for element transfer in subduction zones, Lithos, 92, 399–417, 2006a.

Hermann, J., Rubatto, D., Korsakov, A. V., and Shatsky, V. S.: The age of metamorphism of diamondiferous rocks determined with SHRIMP dating of zircon, Russ. Geol. Geophys., 47, 511–518, 2006b.

Hovis, G. L., Tribaudino, M., Altomare, C., and Bosi, F.: Thermal expansion of minerals in the tourmaline supergroup, Am. Mineral., 108, 1053–1063, 2023.

Kaminsky, F. V., Zakharchenko, O. D., Griffin, W. L., Channer, D. M. D., and Khachatryan-Blinova, G. K.: Diamond from the Guaniamo area, Venezuela, Canad. Mineral, 38, 1347–1370, 2000.

Katayama, I., Maruyama, S., Parkinson, C. D., Terada, K.. and Sano, Y.: Ion micro-probe U-Pb zircon geochronology of peak and retrograde stages of ultrahigh-pressure metamorphic rocks from the Kokchetav massif, northern Kazakhstan, Earth Planet. Sc. Lett., 188, 185–198, 2001.

Korsakov, A. V., Shatsky, V. S., Sobolev, N. V., and Zayachkovsky, A. A.: Garnet-biotite-clinozoisite gneisses: a new type of diamondiferous metamorphic rocks of the Kokchetav massif, Eur. J. Mineral., 14, 915–929, https://doi.org/10.1127/0935-1221/2002/0014-0915, 2002.

Korsakov, A. V., Travin, A. V., Yudin, D. S., and Marschall, H. R.: 40Ar/39Ar dating of tourmaline from metamorphic rocks of the Kokchetav massif, Kazakhstan, Dokl. Earth Sci., 424, 168–170, 2009.

Korsakov, A. V., Yudin, D. S., Musiyachenko, K. A., and Demin, S. P.: $^{40}Ar/^{39}Ar$ dating of maruyamaite (K-dominant tourmaline) from diamond-bearing metamorphic rocks from the Kokchetav massif, Geodyn. Tectonophys., 14, 0699, https://doi.org/10.5800/GT-2023-14-3-0699, 2023a (in Russia).

Korsakov, A. V., Mikhailenko, D. S., Zhang, L., and Xu, Y.: Inclusions of diamond crystals in the tourmaline of the schorl-uvite series: problems of genesis, J. Min. Inst, 264, 833–841, https://pmi.spmi.ru/pmi/article/view/16082/16081, 2023b.

Korsakov, A. V., Musiyachenko, K. A., Mikhailenko, D. S., and Demin, S. P.: Origin of potassium-bearing tourmalines of the Kumdy-Kol deposit (Kokchetav massif, Northern Kazakhstan): Mineral inclusions study, Lithosphere, 23, 500–514, 2023c.

Lavrova, L. D., Pechnikov, V. A., Pleshakov, M. A., Nadezhidina, E. D., and Shukolyukov, Y. A.: A new genetic type of diamond deposit, Scientific World Publishing House, Moscow, Russia, https://doi.org/10.1017/CBO9780511573088, 1999.

Likhacheva, A. Y., Rashchenko, S. V., Musiyachenko, K. A., Korsakov, A. V., Collings, I. E., and Hanfland, M.: Compressibility and structure behaviour of maruyamaite (K-tourmaline) from the Kokchetav massif at high pressure up to 20 GPa, Mineral. Petrol., 113, 613–623, 2019.

Lussier, A., Ball, N. A., Hawthorne, F. C., Henry, D. J., Shimizu, R., Ogasawara, Y., and Ota, T.: Maruyamaite, $K(MgAl_2)(Al_5Mg)Si_6O_{18}(BO_3)_3(OH)_3O$, a potassium-dominant tourmaline from the ultrahigh-pressure Kokchetav massif, northern Kazakhstan: Description and crystal structure, Am. Mineral., 101, 2, 355–361, 2016.

Marschall, H. R., Korsakov, A. V., Luvizotto, G. L., Nasdala, L., and Ludwig, T.: On the occurrence and boron isotopic composition of tourmaline in (ultra)high-pressure metamorphic rocks, J. Geol. Soc., 166, 811–823, 2009.

Mikhailenko, D., Golovin, A., Korsakov, A., Aulbach, S., Gerdes, A., and Ragozin, A.: Metasomatic Evolution of Coesite-Bearing Diamondiferous Eclogite from the Udachnaya Kimberlite, Minerals, 10, 383, https://doi.org/10.3390/min10040383, 2020.

Mikhailenko, D. S., Aulbach, S., Korsakov, A. V., Golovin, A. V., Malygina, E. V., Gerdes, A., Stepanov, A. S., and Xu, Y. G.: Origin of Graphite–Diamond-Bearing Eclogites from Udachnaya Kimberlite Pipe, J. Petrol., 62, 1–32, 2021.

Musiyachenko, K. A., Korsakov, A. V., Shimizu, R., Zelenovskiy, P. S., and Shur, V. Y.: New insights on Raman spectrum of K-bearing tourmaline, J. Raman Spectrosc., 51, 1415–1424, 2020.

Musiyachenko, K. A., Korsakov, A. V., and Letnikov, F. A.: A New Occurrence of Maruyamaite, Dokl. Earth Sci., 498, 403–408, 2021.

O'Bannon, E., Beavers, C. M., Kunz, M., and Williams, Q.: High-pressure study of dravite tourmaline: Insights into the accommodating nature of the tourmaline structure, Am. Mineral., 101, 1622–1633, 2018.

Ota, T., Kobayashi, K., Katsura, T., and Nakamura, E.: Boron cycling by subducted lithosphere; insights from diamondiferous tourmaline from the Kokchetav ultrahigh-pressure metamorfic belt, Geochim. Cosmochim. Ac., 72, 3531–3541, 2008.

Papike, J. J.: Pyroxene mineralogy of the Moonand meteorites, in: Pyroxenes, edited by: Prewitt, C. T., Mineralogical Society of America, Washington D.C., Rev. Mineral. Geochem., 7, 495–525, 1980.

Pesquera, A., Gil-Crespo, P. P., Torres-Ruiz, F., Torres-Ruiz, J., and Roda-Robles, E.: A multiple regression method for estimating Li in tourmaline from electron microprobe analyses, Mineral. Mag., 80, 1129–1133, 2016.

Pokhilenko, N. P., Sobolev, N. V., Reutsky, V. N., Hall, A. E., and Taylor, L. A.: Crystalline inclusions and C-isotope ratios in diamonds from the Snap Lake/King Lake kimberlite dyke system: evidence of ultradeep and enriched litospheric mantle, Lithos, 77, 57–67, 2004.

Pouchou, J. L. and Pichoir, F.: Quantitative analysis of homogeneous or stratified microvolumes applying the model "PAP", Electron Probe Quantification, Plenum Press, New York, edited by: Heinrich, K. F. J. and Newbury, D. E., Plenum, New York, 31–75, https://doi.org/10.1007/978-1-4899-2617-3_4, 1991.

Prinz, M., Mansoni, D. V., Hlava, P. F., and Keil, K.: Inclusions in diamonds: garnet lherzolite and eclogite assemblages, Phys. Chem. Earth, 9, 797–815, 1975.

Robinson, K., Gibbs, G. V., and Ribbe, P. H.: Quadratic elongation: a quantitative measure of distortion in coordination polyhedra, Science, 172, 567–570, 1971.

Safonov, O. G., Bindi, L., and Vinograd, V. L.: Potassium-bearing clinopyroxene: a review of experimental, crystal chemical and thermodynamic data with petrological applications, Mineral. Mag., 75, 2467–2484, 2011.

Seki, Y. and Kennedy, G. C.: The breakdown of potassium feldspar, $KAlSi_3O_8$ at high temperatures and high pressures, Am. Mineral., 49, 1688–1706, 1964.

Shatsky, V. S., Sobolev, N. V., and Vavilov, M. A.: Diamond-bearing metamorphic rocks of the Kokchetav massif (northern Kazakhstan), in: Ultra-High Pressure Metamorphism, Cambridge University Press, 427–455, 1995.

Shatsky, V. S., Jagoutz, E., Sobolev, N. V., Kozmenko, O. A., Parkhomenko, V. S., and Troesch, M.: Geochemistry and age of ultrahigh pressure metamorphic rocks from the Kokchetav massif (Northern Kazakhstan), Contrib. Mineral. Petrol., 137, 185–205, 1999.

Shimizu, R. and Ogasawara, Y.: Discovery of "K-tourmaline" in Diamond-Bearing Tourmaline-K-Feldspar-Quartz Rock From the Kokchetav Massif, Kazakhstan, AGU Fall Meeting Abstracts, 2005.

Shimizu, R. and Ogasawara, Y.: Diversity of potassium-bearing tourmalines in diamondiferous Kokchetav UHP metamorphic rocks: A geochemical recorder from peak to retrograde metamorphic stages, J. Asian Earth Sci., 63, 39–55, 2013.

Schmidt, M. W.: Experimental Constraints on Recycling of Potassium from Subducted Oceanic Crust, Science, 272, 1927–1930, 1996.

Sheldrick, G. M.: Crystal structure refinement with SHELXL, Acta Crystallogr. C, 71, 3–8, 2015.

Sobolev, N. V.: Deep-seated inclusions in kimberlites and the problem of the composition of the upper mantle, Washington, D.C., American Geophysical Union, 279 pp., ISBN: 10 0875902022, 13 978-0875902029, 1977.

Sobolev, N. V. and Shatsky, V. S.: Diamond inclusions in garnets from metamorphic rocks: a new environment for diamond formation, Nature, 343, 742–746, 1990.

Sobolev, N. V., Shatsky, V. S., Vavilov, M. A., and Goryainov, S. V.: Coesite inclusion in zircon of diamondiferous gneisses of the Kokchetav massif: the first finding of coesite in metamorphic rocks on the territory of the USSR, Dokl. Akad. Nauk SSSR, 321, 184–188, 1991.

Sobolev, N. V., Yefimovam E. S., Channer, D. M. DeR., Anderson, P. F. N., and Barron, K. M.: Unusual upper mantle beneath Guaniamo, Guyana Shield, Venezuela: evidence from diamond inclusions, Geology, 26, 971–974, 1998.

Stachel, T., Brey, G. P., and Harris, J. W.: Kankan diamonds (Guinea) I: from the litosphere down to the transition zone, Contrib. Mineral. Petrol., 140, 1–15, 2000.

Stepanov, A. S., Rubatto, D., Hermann, J., and Korsakov, A. V.: Contrasting *P-T* paths within the Barchi-Kol UHP terrain (Kokchetav Complex): Implications for subduction and exhumation of continental crust, Am. Mineral., 101, 788–807, 2016.

Theunissen, K., Dobretsov, N. L., Shatsky, V. S., Smirnova, L., and Korsakov, A.: The diamond-bearing Kokchetav UHP massif in Northern Kazakhstan: exhumation structure, Terra Nova, 12, 181–187, 2000a.

Theunissen, K., Dobretsov, N. L., Korsakov, A., Travin, A., Shatsky, V. S., Smirnova, L., and Boven, A.: Two contrasting petrotectonic domains in the Kokchetav megamelange (north Kazakhstan): difference in exhumation mechanisms of ultrahigh-pressure crustal rocks, or a result of subsequent deformation?, Isl. Arc, 9, 284–303, 2000b.

Thomsen, T. B. and Schmidt, M. W.: Melting of carbonated pelites at 2.5–5.0 GPa, silicate–carbonatite liquid immiscibility, and potassium–carbon metasomatism of the mantle, Earth Planet. Sc. Lett., 267, 17–31, 2008.

Urakawa, S., Kondo, T., Igawa, N., Shimomura, O., and Ohno, H.: Synchrotron radiation study on the High-Pressure and High-

Temperature phase relations of $KAlSi_3O_8$, Phys. Chem. Mineral., 21, 387–391, 1994.

van Hinsberg, V. J., Henry, D. J., and Marschall, H. R.: Tourmaline: an ideal indicator of its host environment, Can. Mineral., 49, 1–16, 2011.

Walenta, K. and Dunn, P. J.: Ferridravite, a new mineral of the tourmaline group from Bolivia, Am. Mineral., 64, 945–948, 1979.

Wang, W. and Takahashi, E.: Subsolidus and melting experiments of a K-rich basaltic composition to 27 GPa: Implication for the behavior of potassium in the mantle, Am. Mineral., 84, 357–361, 1999.

Yagi, A., Suzuki, T., and Akaogi, M.: High pressure transition in the system $KAlSi_3O_8$-$NaAlSi_3O_8$, Phys. Chem. Mineral., 21, 12–17, 1994.

Žáček, V. and Hyršl, P.: Chemistry and origin of povondraite-bearing rocks from Alto Chapare, Cochabamba, Bolivia, J. Czech Geol. Soc., 43, 59–68, 1998.

Žáček, V., Fryda, J., Petrov, A., and Hyršl, J.: Tourmalines of the povondraite – (oxy)dravite series from the cap rock of meta-evaporite in Alto Chapare, Cochabamba, Bolivia, J. Czech Geol. Soc., 45, 3–12, 2000.

Zonenshain, L. P., Kuzmin, M. I., Natapov, L. M., and Page, B. M.: Geology of the USSR: A Plate-Tectonic Synthesis, Am. Geophys. Union., 21, 242 pp., https://doi.org/10.1029/GD021, ISBN: 10 0875905218, 13 978-0875905211, 1990.